Joshi, Shailesh V. and Rowe, Philip J. (2017) A novel approach of intra-operative shape acquisition of the tibio-femoral joints using 3D laser scanning for computer assisted orthopaedic surgery. International Journal of Medical Robotics and Computer Assisted Surgery. ISSN 1478-5951 , http://dx.doi.org/10.1002/rcs.1855

A Novel Approach for Intra-Operative Shape Acquisition of the Tibio-Femoral Joints Using 3D Laser Scanning in Computer Assisted Orthopaedic Surgery

Shailesh V. Joshi, Philip J. Rowe

Department of Biomedical Engineering, University of Strathclyde, Glasgow, G4 0TD, UK

Primary email: joshi.shailesh87@gmail.com
Co-author email: philip.rowe@strath.ac.uk

Address: Department of Biomedical Engineering, University of Strathclyde, Wolfsan, 106 Rottenrow, Glasgow, G4 0TD, UK

Telephone: Dr Shailesh V Joshi: 07532058114

Source of financial support: This study was funded by International fees only studentship from the University of Strathclyde.

Category: Original article

Word count: 5082; 6192 (including reference list)

Number of figures: 8

Number of tables: 3

Abstract

Background:

Image registration (IR) is an important process of developing a spatial relationship between pre-operative data and physical patient in the operation theatre. Current IR techniques for Computer Assisted Orthopaedic Surgery (CAOS) are time consuming and costly. There is a need to automate and accelerate this process.

Methods:

Bespoke quick, cost effective, contactless and automated 3D laser scanning techniques based on the DAVID Laserscanner method were designed. 10 cadaveric knee joints were intra-operatively laser scanned and were registered with the pre-operative MRI scans. The results are supported with a concurrent validity study.

Results:

The average absolute errors between scan models were systematically less than 1 mm. Errors on femoral surfaces were higher than tibial surfaces. Additionally, scans acquired through the large exposure produced higher errors than the smaller exposure.

Conclusion:

This study has provided proof of concept for a novel automated shape acquisition and registration technique for CAOS.

Introduction

Osteoarthritis (OA) is one of the most common musculoskeletal diseases affecting around 8.75 million of the population in UK[1]. It is a chronic joint disorder characterised by degeneration of the articular cartilage which results in a severe pain while performing daily voluntary musculoskeletal activities. The knee joint is the most common site to be affected by OA and 4.7 million people in the UK had OA of knee in 2010. This is estimated to rise to 5.4 million by 2020[1].

After non-surgical treatments have been exhausted, patients suffering from OA of the knee are usually advised to undergo knee replacement surgery where the articulating surfaces of the tibio-femoral joint are resected and are replaced with prosthetic implants. Recently, knee replacement surgery has been increasingly supported using the computers (Computer Assisted Orthopaedic Surgery (CAOS)) along with advanced robotic systems. CAOS robotic procedures such as MAKOplasty® typically comprise of three main phases: 1) Pre-operative planning; 2) Intra-operative execution; and 3) Implant placement. Pre-operatively, high resolution DICOM (Digital Imaging and Communications in Medicine) scans of the patient’s knee joint are acquired which are then used to plan the surgery. Based on this plan, intra-operatively the surgery is performed with the help of computer navigation and robotics. Finally, the implant prosthesis is precisely placed and its position is monitored with the navigation system.

In most CAOS applications for knee surgery, pre-operative CT scans are acquired on the patient’s leg and are segmented to create a patient specific 3D knee model. Image registration (IR) is one of the important intra-operative phases of CAOS in which a spatial relationship between the pre-operative imaging data and the physical patient present in the operation theatre is developed. IR in most CAOS knee surgery applications is achieved using a manual method comprising hand-held navigated probes. Anatomical points are acquired by physically touching the probe over the articulating surfaces (tibial plateaux and femoral condyles) of the knee joint to form a point cloud which can then be fitted to the pre-operative scan data using a best fit type minimisation. However, this manual digitisation approach is laborious, time consuming and hence costly. In our recent surgical trial of MAKOplasty®[2] this process consumed upwards of 14-20 minutes[3].

Study Design

In this study, a bespoke automated and contactless 3D laser scanner was built and used to acquire the point clouds of the articulating surfaces of the cadaveric knee joints. In the first concurrent validity, the laser and MRI scanned data of the cadaveric knee joints was compared to establish the accuracy and reliability of the laser scanning technique.

In addition, a supplementary validity study was conducted for every cadaveric sample in which the distance measurements acquired by the laser scanner were assessed against standard digital vernier calliper measurements.

Materials and Methods

10 fresh frozen cadaver knee joints were used in the study. Eight out of the ten samples were obtained from the Anatomy Gift Registry, 7522 Connelley Drive, Suite L, Hanover, MD 21076, USA. The remaining two samples were collected from the Clinical Anatomy Skills Centre (CASC), Glasgow University, Glasgow, UK. All the samples were stored in the freezer at -19.5 °C and had their anatomical structure present from hemi-pelvis to toe.

Prior to these studies, all cadaver legs had been operated on post donation with a medial UKA surgery. Lateral compartments of all the samples were intact with smooth articular cartilage which were used in this investigation.

Concurrent Validity Study 1:

The surface topology of the cartilage surfaces was experimentally acquired using 3D FLASH (Fast Low Angle Shot) MR imaging technique. This technique is used clinically and provides high signal to noise ratio (SNR) and contrast to noise ratio (CNR) to adequately set apart cartilage and bone interfaces in healthy as well as arthritic knee joints[4, 5]. Although, 3D FLASH MR imaging provides poor contrast between synovial fluid and cartilage and high sensitivity to the artefacts; the technique still makes the segmentation of the articular cartilage and bone relatively easier and is still therefore considered the standard MR imaging technique for depicting articular cartilage morphology [4-8].

All the samples were thawed 48 hours prior to the MR imaging and were scanned on a Siemens MRI station at 1.5 T using 3D FLASH technique. A standard protocol presented in the literature was followed[4, 5, 9]. The slice thickness was 1 mm with no gap width. With a field of view (FOV) of 160 mm, flip angle of 12° was set at 0.3 mm X 0.3 mm in plane resolution and 512 X 512 acquisition matrix. The protocol was approved by a highly skilled clinical imaging research team in the Western Infirmary, Glasgow where the scanning was performed. A sagittal MRI was performed (figure 1) and the scan slices were converted into a 3D volume. Samples were placed in the freezer post MRI scanning.

Figure 1: A sample MRI scan of the right knee joint

DICOM MRI images were segmented using advanced clinical software Mimics (Materialise's Interactive Medical Image Control System) designed for medical image processing. 3D point clouds of the articular cartilage surfaces were generated and were exported in binary. STL (Stereolithography) format using the STL+ module.

For the laser scanning, a low cost range scanner was constructed using basic components such as a calibration mask, a camera and a laser source[10]. Winkelbach and co-authors[11] provided a real-time self-calibrating hand-held 3D laser scanning system, which is now also known as DAVID Laserscanner. This system is free from markers and uses sub-pixel analysis of greyscale difference images. This method works with a fast surface registration and with an improved random surface matching process based on the RANSAC (Random Sample Consensus) algorithm[12]. This approach is not only robust and efficient but also can match frames of objects without the need for an initial guess of the position.

Using the typical DAVID Laserscanner software package, scanning can be achieved with satisfactory accuracy and precision; but, the calibration planes need to be placed behind the object at all times during scanning. Due to the complexity in the knee joint and its positioning in the theatre, keeping the calibration curves behind the knee during scanning would be highly impractical. Moreover, hand-held scanning could be further time consuming due to irregularities in the manual movement by human arm. However, more recent versions of the software enable users to perform the scanning without calibration planes; provided that the laser source is moved in a precise constant motion and the relative distance between the receiving camera and the laser source remains fixed at all times. Thus, the scanner developed using DAVID Laserscanner was automated to eliminate the use of calibration planes during actual scanning.

After an extensive review of the relevant literature, possible laser emitters of suitable wavelength and power output were found which could generate a safe and undistorted output[13-17]. A low cost (£3) class 2 line laser module (1 mW, 650 nm) was interfaced with a standard Logitech 720p detector webcam costing £17. The laser source was attached to the shaft of a geared bipolar stepper motor using a bespoke machined T-joint slot. A2 sized calibrations planes were used for the calibration and were then removed for the actual scanning.

The laser emitter (attached to the geared stepper) and the detector camera were mounted on a robust positioner assembly constructed using Aluminium extrusion plates (figure 2 (a)). In addition, the scanning modules were mounted on the end-effector of the MAKO Surgical Corps's RIO® arm shown in the figure 2(b). This mimics the setup which would be possible if this robotic surgical system was in use during MAKOplasty® surgery.

Figure 2: 3D Laser scanner (a): Scanner mounted on the aluminium extrusion framework (b): Laser scanner mounted on the joint six of the MAKO RIO® arm

Each cadaveric leg sample was again thawed 48 hours prior to the experiments. The samples were attached to a surgical table in a typical knee flexed operating position using straps around the hemi-pelvis as shown in the figure 3. The foot was attached to a sliding foot holder to allow variable knee flexion. The scans for each leg were acquired using two setups (Aluminium extrusion and RIO) to investigate whether there is any difference between the bulky extrusion based scanner and a more portable RIO mounted scanner. In addition, two typical surgical exposures (UKA, TKA) were used as variables.

Figure 3: Sample cadaver set up on the bed with the attached arrays for MAKO registration

The laser scans were post processed using a robust digital image software package, Geomagic Qualify®12. This software is certified and has received very high accuracy certification from widely accepted organisations such as Physikalisch-Technische Bundesanstalt (PTB) institute and National Institute of Standards and Technology (NIST) in the area of least squared surface and curve fitting (Accurate up to 0.1 μm in length and 0.1" [1/36,000 of a degree] in angle)[18].

Each laser scan (test) was first visually aligned using manual registration with the segmented MRI (reference) (figure 4) by selecting 3 to 9 common points on each surface. This is a type of surface registration (point based registration or free-form surface matching) that works closely on the Iterative Closet Point (ICP) algorithm where the two surfaces are aligned with respect to the closest points leading to the segments and the triangles[19-21]. Thus, manual registration adjusts spatial position of the floating scan using position of the fixed scan based on the user-defined pairs of corresponding points from each scan.

Figure 4: Manual registration by selecting random points over the left lateral tibial surface (a): MRI generated 3D model (red) of the articular cartilage, set as a reference model. (b): Corresponding 3D laser scan (green) of the same cartilage acquired intra-operatively, set as a test model. (c): Rough manual registration between two surfaces

After approximate manual registration, global registration was performed where the alignment between the models is automatically fitted using ICP algorithm based on their spatial position. Here, the fixed and floating scans are both moved around slightly to find the best alignment possible. After this rough registration, reference and test models were aligned using ICP based automatic best fit type of minimisation to produce a fine-tuned fit in order to evaluate absolute errors between scans. In this alignment stage, test (laser) scan is sampled and the closest points are computed to each point on the reference scan, based on the selected sample size. Using the least-squares method, the sums of squares of distances between the sample pairs are evaluated which are minimized over all the rigid motions that could realign the two objects. Having done this, the closet points are re-computed on the reference to establish a new transformation matrix. With the results of the fit, average absolute errors (AAE) between the models were calculated. Each deviation is a Euclidean distance in a 3D space between the two closest points. 3D color-coded mappings of residual differences between the scans were then generated to visualise the spatial distribution of the errors.

In the experimental design, three independent variables were used each with two levels viz., the exposure (UKA, TKA), the positioner setup (Aluminium assembly, MAKO RIO), and type of the surface (tibia, femur). A Repeated measures ANOVA test was performed using a standard statistical software package, SPSS (developed by IBM Corporation, NY, USA) to investigate the effects of the independent variables on the dependent variable (AAE).

Validity Study 2:

At the end of the scanning session for each sample, cadaver legs were employed in the subsequent validity study where the Euclidean distance measurements acquired using 3D laser scanner were compared with the standard digital vernier callipers measurements. Tibial and femoral articulating condyles were treated as separate surfaces thereby providing 20 set of surfaces. On each surface, 7 M2 screws were inserted in a random pattern but with a good spread as shown in figure 5(a). The distances between the centres of each screw with the centres of every other screw were measured thus providing 21 different distance measurements on each surface as shown in figure 5(b). The 21 measurements for each of the 20 surfaces resulted in 21*20 = 420 different measurements. For every surface, 10 laser scans were acquired. Thus, in total 4200 distance measurements acquired from laser scans were compared with the corresponding digital vernier calliper measurements.

Figure 5: Distance measurements between the screw markers on the tibial condyle (a): Placement of seven screws over the surface (b): Total number of measurements (21) computed between every pair of the points (c): Direct distance measurement acquired using digital vernier calliper (d): Distance measurement (in the white box) acquired on the corresponding digitised 3D laser scan and formulated using Geomagic Qualify®

The laser scans were analysed in Geomagic Qualify® 12 in which the distances between the pairs of screws were evaluated using the distance calculation tool based on the Euclidean metric calculation in the 3D space (figure 5(d)).

For every set of measurements, an absolute error (AE) and absolute percent error (APE) were computed followed by average absolute error (AAE) and average absolute percentage error (AAPE, also known as MAPE, mean absolute percentage error). Significance in both studies was tested at α=0.05 level.

Results

The key findings of the studies are reported in this paper. The in-depth investigation is available online[10]. The outcome of the data comparison for a single femoral scan example is explained in detail with its deviation distribution and spatial distribution of the deviations in a colour coded pattern. This is followed by a summary table of all the samples.

This particular example (figure 6 and 7) shows a comparison between MRI and the laser scan of the right femoral lateral cartilage. The AAE[*] of 0.21 mm was reported with SD_{AE}[*] of 0.32 mm. The $+d_{max}$[*] and $-d_{max}$[*] were 1.88 mm and -1.38 mm respectively.

Figure 6: Deviation distribution between MRI and laser scan of an example right femoral lateral cartilage

Deviation in mm is plotted against the percentage of points within the range of deviations. Note: $\pm d_{max}$ occurred at the periphery

[*] AAE: Average absolute error, SD_{AE}: Standard deviation of the absolute error, $+d_{max}$: Maximum positive deviation, $-d_{max}$: Maximum negative deviation

Figure 7: Top view of the colour deviation map showing spatial distribution of the deviations between MRI and laser scan of right femoral lateral cartilage

The posterior and superior condylar region is clipped as the laser scan was acquired with a minimal exposure (90 mm, mimicking UKA). Note: Large errors ($\pm d_{max}$) at the periphery of the scan

Table 1: Summary of the alignment statistics between MRI and laser scans of femoral surfaces of all the samples

AAE; average absolute error between the models, SD_{AE}; standard deviation of the absolute error, $+d_{max}$ and $-d_{max}$; maximum positive and negative deviations respectively. Average and standard deviation of all the parameters is shown at the bottom of the table. Note: d_{max} values occurred at the periphery of the scan zones

Table 2: Summary of the effects of the independent variables on AAE between MRI and laser scans

The main and interaction effects of the independent variables indicating the P-value statistics, the significance of the statistics and the interpretation of the results

Effects of independent variables:

In the next stage, the effects of three independent variables i.e. type of setup (Aluminium extrusion, RIO), type of exposure (UKA, TKA) and type of surface (Tibia, Femur) on the dependent variable, AAE were studied. The main effects of the independent variables as well as the interactions between the variables were studied. The summary of this analysis is reported in table 2.

Validity Study

A bar graph (figure 8(a) and 8(b)) along with error bars depicting variations in the measurements is shown for one of the 20 surfaces. In addition, a summary of all the 4200 measurement comparisons is reported in table 3. Both the methods (laser and vernier calliper) were responsive so changing the differences between the screws and inter measurement system differences were small with 95% of the scanned measurements within 1 mm of the vernier callipers.

Figure 8: Bar graph comparison for the distance calculations between vernier calliper and 3D laser scans

(a): Bar graph for first 11 pairs of screws. (b): Bar graph for remaining 10 pairs of screws

Note: Blue bar is the measurement recorded by the vernier calliper, whereas red bar is the mean value of the measurements on the laser scans. Error bars indicate the range of values (minimum and maximum values). All the measurement differences between vernier calliper and laser were statistically not significant; P>0.05

Table 3: Summary of the assessment of the distance calculations performed using direct measurements (vernier calliper) and the 3D laser scans

AAE; average absolute error between measurements, SD_{AE}; standard deviation of the absolute error, AAPE; average absolute percentage error, SD_{APE}; standard deviation of the absolute percentage error. Average and standard deviation of all the parameters is shown at the bottom of the table. Note: NS= Not significant. All the measurement differences between vernier calliper and laser were statistically not significant; P>0.05

Discussion

Over the last decade, CAOS has emerged particularly in the area of minimally invasive UKA surgery. With the more conservative approach of UKA (as compared to TKA), which have been reenergised with the development of the advanced robotic systems, only the affected compartment (medial/lateral) is resected and an implant is placed to facilitate normal joint function. One of the most important phases of the computer assisted surgical process in the operating theatre is to develop a spatial relationship between the pre-operatively acquired patient specific scan of the knee surface and the physical patient knee present in the operating theatre. It is possible to visualise key anatomical points around the patient's knee joint in the CT/MRI scan as well as to locate the same points on the actual patient during surgery using intra-operative sensors or probes. However, their spatial correspondence remains unknown until IR is achieved. IR is the process that generates the relationship between the scan and the patient and allows the surgeon to visualise the 3D pre-operative scan data in-relation to the patient's anatomy in the operating theatre. It is therefore a crucial aspect of the procedure. This study demonstrates a novel laser scanning technique which is proposed as an alternative to the current time consuming IR methods in knee CAOS. Laser based registration can be achieved in less than half the time used in the manual technique which can save time in the theatre and thus cost[41].

An example showing detailed comparison between MRI and corresponding laser scan of the cadaveric femoral condyle has been presented (figure 6 and 7). The average deviation (AAE) between the laser and MRI scans was 0.32 mm with a standard deviation (SD_{AE}) of 0.32 mm. The maximum positive ($+d_{max}$) and negative ($-d_{max}$) deviations were +1.88 mm and -1.38 mm respectively. The total number of point pairs used for the data comparison was 5266 out of which 98.48% were within ±0.94 mm of deviation. Moreover, in figure 7, it can be clearly seen that the absolute errors tend to increase as the extreme edges of the scan area are approached. The tibial surfaces and rest of the femoral surfaces showed a similar trend with maximum % of deviations within ±1 mm and higher errors towards peripheries. Summary of the alignment statistics between MRI and laser scans of femoral surfaces for all the samples is shown in table 1.

The effects of independent variables (setup, exposure and surface) were investigated using repeated measures ANOVA and are shown in table 2. There was no statistically significant difference on AAE within two types of setups (Al and RIO), $F(1,9) = 1.148$; $P=0.312$ which indicates that the bulky Aluminium extrusion setup can be replaced with the positioning RIO arm which in our case would be already present in the theatre. Thus, it would be possible to make one compact system consisting of the robot and the scanner and save plenty of space in the operating theatre. The AAE with TKA exposure was significantly higher than UKA exposure, $F(1,9) = 40.808$; $P= 0.0001$. It may seem that greater errors occurred with greater exposure but this was a result of exposing more edges to the scan where the surface was at a greater angle to the incident laser light and hence, the errors in depth perception possibly produced larger errors between the laser scan and the MRI images. However, these errors remained sub-millimetric. The AAE on the femoral surfaces was significantly higher than on the tibial surfaces, $F(1,9) = 14.863$; $P = 0.004$. The ends of the femoral condyles contain more regions where the profile of the bone surface is at a greater angle to the incident laser light and hence higher errors at the peripheries contribute to overall higher AAE. However, these errors were again sub-millimetric. In other words, the higher errors with TKA exposure (as compared with UKA exposure) and on femoral surfaces (as compared to tibial surfaces) can be attributed to the 'edge effect' which affects most triangulation systems. It can be seen in the colour coded deviation distribution map (figure 7) where the higher % of the larger deviations appeared on the peripheries. 3D scanners and particularly laser based scanners tend to produce errors at the spatial discontinuities or edges of the surfaces being scanned. When the laser hits the surface edges, only a certain part is reflected from the actual point and some reflection is always induced by the adjacent surfaces or the surface behind the object. Thus, the final signal is a mixture of the signals from the foreground and the background. This phenomenon is called a 'mixed-pixel effect' or 'edge effect'. Due to the higher slope on the edge of the surface and the viewing direction of the scanner, the laser plane falls almost tangentially on the edge which leads to errors in location of these points in the cloud and thus causes inaccuracies and distortions in the scan[22-28].

During the scanning, the scanner was always positioned such that the surface (tibial and femoral condyle) being scanned was in the centre of the camera image. With the TKA incision, additional surface exposure is provided which is usually towards the peripheral region of the surface. Also, femoral condyles are more non-uniform and curved in their surface topography when compared to the tibial plateau. So, while scanning the femoral condyles, there is a higher slope of the target around the edges and the curved region which causes higher deviations in those areas. As a result, the laser plane incidents more tangentially on the femoral condyles as compared to the tibial plateau and thus the edge effect results in higher deviations.

Furthermore, a careful statistical investigation showed that there was no significant interaction (two-way and three-way) found between the variables. As the interactions were not significant, the main effects of the independent variables can be accepted[29-32].

The second stage in the experimental design was to compare the automated distance measurements acquired using the developed laser scanner with the manual measurements from digital vernier calliper, an approach widely accepted in research and industry to evaluate the technical performance of 3D imaging system for geometric accuracy[33-40]. A bar graph with error bars for an example surface is presented in figures 8(a) and 8(b). The rest of the surfaces followed a similar pattern. The error bars indicate the range (minimum and maximum) of the reported values. The AAE values ranged from 0.3 mm to 0.62 mm with a mean of 0.46 mm and SD of 0.08 mm. The SD_{AE} within each surface was 0.15 mm. Furthermore, for every set of data, AAPE was reported which ranged from 1.19% to 2.45% with the mean of 1.66% and SD of 0.31%. The mean standard deviation of AAPE within each surface (SD_{AAPE}) was 0.82% with SD of 0.24% and min/max values of 0.54% and 1.40%. The measurements between two systems were analysed using two sample independent t-test[35]. The P-values for each surface comparison are reported in table 3. None of the differences were statistically significant, $P>0.05$ and in fact the P-values were very close to 1. Hence, we conclude that there is no sufficient evidence to suggest that laser readings and vernier calliper distance measurements were different. The mean of the deviations (Mean AAE) for all the 20 surfaces was less than 0.5 mm (0.46 mm) with an average SD_{AE} of 0.15 implying that 95% of the deviations (4200 measurements) lay within 0.46±0.3 (2 SD) i.e. within 0.16-0.76 mm absolute deviation which is suitable for orthopaedic surgeries.

Limitations and future recommendations

3D laser scanners have obvious advantages such as high speed, accuracy, precision and reproducibility. However, their strength can be affected by various factors. Stray light or an unidentified light source can affect the quality of the scans. Thus, care must be taken to avoid such sources and most importantly any proximal light source which might enter the triangulation plane i.e. the plane formed by camera, laser source and object being scanned. Shadow of the surrounding structures can produce gaps in the scans. Due to the awkward and complex structure of the tibio-femoral joint, femoral condyles may produce occultation on tibial plateaux. Further safely flexing the knee joint can enable the user to acquire maximum exposed area. Also, to avoid possible hindrance, the skin surrounding the incision needs to be retracted, especially in the smaller UKA exposures to allow the detector camera to completely visualise the area (condyles) under scrutiny.

A simple way of controlling the edge effect would be by removing any regions where the slope of the scan is at an acute angle to the scanner as these are the areas that are most likely to add higher magnitude of errors to the fitting. An automated process is thus required as manually removing the edges would add additional time in the data post-processing phase in theatre. For the validity study, inter-operator variation was eliminated but intra-operator variation should be investigated by repeating the same measurement of the digital vernier calliper acquired by the same operator to check the variation.

This project focussed on acquiring accurate 3D surface geometry of tibio-femoral joints in the theatre. Optically navigating the scanner in real time was beyond the scope of this project. However, as the next stage of the project, the laser line could be navigated using geometrical principles and with use of marker frame which are tracked by the IR cameras already utilised in the surgery. Once this is achieved, it could be possible to plan and execute the surgery in theatre there and then. This imageless navigation would be very effective in terms of reduced cost, time and radiation dosage and would provide convenience to patients and clinicians. The proof of concept in real surgery is still to be obtained and is the next step in the process towards a suitable medical device which can be used in the general surgery.

Commercially available high precision laser lines and high-speed CMOS wireless cameras could be used instead of the scanning components used in the study and would further improve the accuracy of the scans and reduce the acquisition time. Further scanning of more cadaver legs should be undertaken and more independent variables should be explored such as distance between centre of the scanner and surface being scanned, sex of the patient, cross sectional area of the surface, etc.

Conclusion

A series of experiments in this study demonstrated that average deviations between the MRI and the 3D laser scans were in general less than half a millimetre. This suggests that the system can repeatedly acquire accurate 3D scans of the tibio-femoral cartilage and bone and in-situ in the operating theatre environment. The second validity study has proven that the developed laser scanner measurements were accurate, precise and repeatable as compared to the standard measurement system such as digital vernier calliper. The sample size of 10 surfaces should be born in mind with the sub-millimetric accuracy of the scans.

This study has addressed an important issue of replacing the current manual intra-operative surface acquisition and image registration process of CAOS with 3D laser scanning. In this study, the feasibility of using an automated 3D scanner based on the DAVID laser scanning technique was validated. The system is capable of acquiring scans of the tibio-femoral joints in theatre to generate complete 3D models of the surface geometry and to an accuracy less than 1 degree across the whole scan surface. The proposed technique is completely contactless and does not require critical points in the hidden regions of the joint thereby allowing surgeons to control the overall incision size limited to the surface being burred. The system was built using inexpensive components and the total cost of the scanning hardware was less than £200. Using the MAKO Surgical registration approach to register each bone surface required approximately 15 minutes whereas the overall time for proposed laser based registration was less than 4 minutes for every joint out of which majority of the time was spent in the post processing of scans which could further be automated.

The system and method have much to offer to CAOS in terms of speed and accuracy of registration and also the potential for both imageless surgery as well as cartilage property assessments.

Acknowledgements

We would like to thank Dr. Philip Riches for arranging the samples and the lab space as well as providing assistance in acquiring the ethical approvals for the experiments. We are thankful to Dr. Gareth Pierce for allowing us to perform pilot studies using the departmental laser scanner. We would also like to thank to the research radiology team of the Western Infirmary, Glasgow for the clinical scanning of the samples.

Competing interests

The authors have no competing interests to disclose.

Table 1: Summary of the alignment statistics between MRI and laser scans of femoral surfaces of all the samples

AAE; average absolute error between the models, SD_{AE}; standard deviation of the absolute error, $+d_{max}$ and $-d_{max}$; maximum positive and negative deviations respectively. Average and standard deviation of all the parameters is shown at the bottom of the table. Note: d_{max} values occurred at the periphery of the scan zones.

	UKA Exposure								TKA Exposure							
	On Al Extrusion				On RIO				On Al Extrusion				On RIO			
Samples	AAE (mm)	SD_{AE} (mm)	d_{max} (mm)		AAE (mm)	SD_{AE} (mm)	d_{max} (mm)		AAE (mm)	SD_{AE} (mm)	d_{max} (mm)		AAE (mm)	SD_{AE} (mm)	d_{max} (mm)	
			+	-			+	-			+	-			+	-
1	0.23	0.33	1.84	-1.50	0.26	0.42	1.51	-1.67	0.28	0.42	1.81	-1.82	0.27	0.44	1.85	-1.94
2	0.20	0.29	2.07	-1.37	0.18	0.28	1.30	-2.03	0.35	0.68	2.15	-2.47	0.33	0.61	2.30	-2.24
3	0.28	0.40	1.49	-1.60	0.28	0.44	1.51	-1.86	0.33	0.46	1.49	-1.69	0.32	0.47	1.87	-1.89
4	0.23	0.33	1.84	-1.50	0.26	0.42	1.51	-1.67	0.28	0.42	1.81	-1.82	0.27	0.44	1.85	-1.94
5	0.21	0.28	1.15	-0.99	0.24	0.33	1.34	-1.31	0.25	0.46	2.73	-2.20	0.27	0.37	2.72	-1.97
6	0.25	0.58	1.43	-1.91	0.25	0.53	1.79	-1.88	0.29	0.66	2.53	-2.20	0.30	0.60	2.46	-2.54
7	0.21	0.31	1.75	-1.39	0.23	0.33	1.72	-1.37	0.28	0.32	1.74	-1.25	0.29	0.38	2.52	-1.46
8	0.26	0.44	1.36	-1.97	0.26	0.46	1.32	-2.19	0.28	0.59	1.97	-3.03	0.30	0.64	2.56	-2.46
9	0.29	0.38	1.23	-1.57	0.28	0.40	1.43	-1.56	0.32	0.45	1.63	-1.73	0.33	0.54	1.93	-2.32
10	0.24	0.36	1.66	-1.65	0.23	0.31	1.31	-1.13	0.30	0.40	2.18	-1.63	0.27	0.40	2.61	-2.50
Average	0.24	0.37	1.58	-1.55	0.25	0.39	1.47	-1.67	0.29	0.48	2.00	-1.98	0.29	0.49	2.27	-2.12
SD	0.03	0.09	0.30	0.28	0.03	0.08	0.17	0.33	0.03	0.12	0.39	0.51	0.03	0.10	0.35	0.35

Table 2: Summary of the effects of the independent variables on AAE between MRI and laser scans

The main and interaction effects of the independent variables indicating the P-value statistics, the significance of the statistics and the interpretation of the results.

Effects	Independent variables	P-value statistics	Significance	Interpretation
Main Effects	Type of Setup (AI, RIO)	$F(1,9) = 1.148$; $P = 0.312$	Not significant	No difference in two types of setup
	Type of Exposure (UKA, TKA)	$F(1,9) = 40.808$; $P = 0.0001$	Significant	Errors slightly larger with TKA exposure
	Type of Surface (Tibia, Femur)	$F(1,9) = 14.863$; $P = 0.004$	Significant	Errors slightly larger on femoral surface
Interaction Effects	Seup*Exposure	$F(1,9) = 0.13$; $P = 0.911$	Not significant	No interaction between setup and exposure
	Setup*Surface	$F(1,9) = 0.474$; $P = 0.509$	Not significant	No interaction between setup and surface
	Exposure*Surface	$F(1,9) = 1.097$; $P = 0.322$	Not significant	No interaction between exposure and surface
	Setup*Exposure*Surface	$F(1,9) = 0.682$; $P = 0.430$	Not significant	No interaction between setup, exposure and surface

Table 3: Summary of the assessment of the distance calculations performed using direct measurements (vernier calliper) and the 3D laser scans

AAE; average absolute error between measurements, SD_{AE}; standard deviation of the absolute error, AAPE; average absolute percentage error, SD_{APE}; standard deviation of the absolute percentage error. Average and standard deviation of all the parameters is shown at the bottom of the table. Note: NS= Not significant. All the measurement differences between vernier calliper and laser were statistically not significant; P>0.05

Surface	AAE (mm)	SD_{AE}	AAPE (%)	SD_{APE}	P-value	Significance
1	0.49	0.17	1.66	0.65	0.930	NS
2	0.61	0.23	2.45	1.40	0.923	NS
3	0.44	0.12	1.66	0.91	0.972	NS
4	0.43	0.14	1.88	1.00	0.987	NS
5	0.48	0.13	1.72	0.63	0.993	NS
6	0.41	0.09	1.49	0.73	0.999	NS
7	0.38	0.13	1.47	0.76	0.992	NS
8	0.47	0.17	1.47	0.62	0.934	NS
9	0.50	0.12	1.55	0.67	0.996	NS
10	0.46	0.11	1.37	0.54	0.993	NS
11	0.49	0.12	1.88	0.80	0.967	NS
12	0.62	0.27	2.17	1.34	0.966	NS
13	0.59	0.23	2.18	0.97	0.986	NS
14	0.47	0.14	1.70	0.82	0.964	NS
15	0.43	0.20	1.50	0.65	0.976	NS
16	0.49	0.25	1.51	0.81	0.965	NS
17	0.39	0.14	1.49	1.10	0.978	NS
18	0.38	0.08	1.40	0.64	0.991	NS
19	0.30	0.09	1.19	0.70	0.974	NS
20	0.43	0.13	1.54	0.67	0.954	NS
Mean	0.46	0.15	1.66	0.82		
SD	0.08	0.05	0.31	0.24		

Figure legends:

Figure 1: A sample MRI scan of the right knee joint

Figure 2: 3D Laser scanner (a): Scanner mounted on the aluminium extrusion framework (b): Laser scanner mounted on the joint six of the MAKO RIO® arm

Figure 3: Sample cadaver set up on the bed with the attached arrays for MAKO registration

Figure 4: Manual registration by selecting random points over the left lateral tibial surface

(a): MRI generated 3D model (red) of the articular cartilage, set as a reference model. (b): Corresponding 3D laser scan (green) of the same cartilage acquired intra-operatively, set as a test model. (c): Rough manual registration between two surfaces

Figure 5: Distance measurements between the screw markers on the tibial condyle (a): Placement of seven screws over the surface (b): Total number of measurements (21) computed between every pair of the points (c): Direct distance measurement acquired using digital vernier calliper (d): Distance measurement (in the white box) acquired on the corresponding digitised 3D laser scan and formulated using Geomagic Qualify®

Figure 6: Deviation distribution between MRI and laser scan of an example right femoral lateral cartilage

Deviation in mm is plotted against the percentage of points within the range of deviations. Note: $\pm d_{max}$ occurred at the periphery

Figure 7: Top view of the colour deviation map showing spatial distribution of the deviations between MRI and laser scan of right femoral lateral cartilage

The posterior and superior condylar region is clipped as the laser scan was acquired with a minimal exposure (90 mm, mimicking UKA). Note: Large errors ($\pm d_{max}$) at the periphery

Figure 8: Bar graph for the comparison for the distance calculations between vernier calliper and 3D laser scans

(a): Bar graph for first 11 pairs of screws. (b): Bar graph for remaining 10 pairs of screws

Note: Blue bar is the measurement recorded by the vernier calliper, whereas red bar is the mean value of the measurements on the laser scans. Error bars indicate the range of values (minimum and maximum values). All the measurement differences between vernier calliper and laser were statistically not significant; $P>0.05$

References

1. UK Ar. Osteoarthritis in General Practice Data and Perspectives 2013 [cited 2015 5 January]. Available from: http://www.arthritisresearchuk.org/arthritis-information/data-and-statistics/osteoarthritis.aspx
2. Jones B, Blyth M, MacLean A, Anthony A, Rowe P, editors. Accuracy of UKA implant positioning and early clinical outcomes in a RCT comparing Robotic Assisted and Manual Surgery. CAOS; 2013. Orlando.
3. Banger M, Rowe P, Blyth M. Time analysis of MAKO RIO UKA procedures in comparison with the oxford UKA. Bone & Joint Journal Orthopaedic Proceedings Supplement. 2013;95(SUPP 28):89-.
4. Kornaat PR, Reeder SB, Koo S, Brittain JH, Yu H, Andriacchi TP, et al. MR imaging of articular cartilage at 1.5T and 3.0T: comparison of SPGR and SSFP sequences. Osteoarthritis and cartilage / OARS, Osteoarthritis Research Society. 2005;13(4):338-44.
5. Eckstein F, Cicuttini F, Raynauld JP, Waterton JC, Peterfy C. Magnetic resonance imaging (MRI) of articular cartilage in knee osteoarthritis (OA): morphological assessment. Osteoarthritis and cartilage / OARS, Osteoarthritis Research Society. 2006;14 Suppl A:A46-75.
6. Recht M, Kramer J, Marcelis S, Pathria M, Trudell D, Haghighi P, et al. Abnormalities of articular cartilage in the knee: analysis of available MR techniques. Radiology. 1993;187(2):473-478.
7. Eckstein F, Charles HC, Buck RJ, Kraus VB, Remmers AE, Hudelmaier M, et al. Accuracy and precision of quantitative assessment of cartilage morphology by magnetic resonance imaging at 3.0T. Arthritis and rheumatism. 2005;52(10):3132-6.
8. Roemer FW, Crema MD, Trattnig S, Guermazi A. Advances in Imaging of Osteoarthritis and Cartilage. Radiology. 2011;260(2):332-54.

9. Stahl R, Krug R, Kelley DA, Zuo J, Ma CB, Majumdar S, et al. Assessment of cartilage-dedicated sequences at ultra-high-field MRI: comparison of imaging performance and diagnostic confidence between 3.0 and 7.0 T with respect to osteoarthritis-induced changes at the knee joint. Skeletal radiology. 2009;38(8):771-83.

10. Joshi S. Intra-Operative Shape Acquisition of Tibio-Femoral Joints Using 3D Laser Scanning for Computer Assisted Orthopaedic Surgery: A Proof of Concept (Thesis). Glasgow: University of Strathclyde; 2015.

11. Winkelbach S, Molkenstruck S, Wahl F. Low-Cost Laser Range Scanner and Fast Surface Registration Approach. In: Franke K, Müller K-R, Nickolay B, Schäfer R, editors. Pattern Recognition. Lecture Notes in Computer Science. 4174: Springer Berlin Heidelberg; 2006. p. 718-28.

12. Fischler MA, Bolles RC. Random sample consensus: a paradigm for model fitting with applications to image analysis and automated cartography. Commun ACM. 1981;24(6):381-95.

13. Marmulla R, Luth T, Muhling J, Hassfeld S. Automated laser registration in image-guided surgery: evaluation of the correlation between laser scan resolution and navigation faccuracy. International journal of oral and maxillofacial surgery. 2004;33(7):642-8.

14. Koo S, Gold GE, Andriacchi TP. Considerations in measuring cartilage thickness using MRI: factors influencing reproducibility and accuracy. Osteoarthritis and cartilage / OARS, Osteoarthritis Research Society. 2005;13(9):782-9.

15. Trinh N, Lester J, Fleming B, Tung G, Kimia B. Accurate Measurement of Cartilage Morphology Using a 3D Laser Scanner. In: Beichel R, Sonka M, editors. Computer Vision Approaches to Medical Image Analysis. Lecture Notes in Computer Science. 4241: Springer Berlin Heidelberg; 2006. p. 37-48.

16. Bowers ME, Trinh N, Tung GA, Crisco JJ, Kimia BB, Fleming BC. Quantitative MR imaging using "LiveWire" to measure tibiofemoral articular cartilage thickness. Osteoarthritis and cartilage / OARS, Osteoarthritis Research Society. 2008;16(10):1167-73.

17. Thiruvenkatachari B, Al-Abdallah M, Akram NC, Sandler J, O'Brien K. Measuring 3-dimensional tooth movement with a 3-dimensional surface laser scanner. American journal of orthodontics and dentofacial orthopedics : official publication of the American Association of Orthodontists, its constituent societies, and the American Board of Orthodontics. 2009;135(4):480-5.

18. Geomagic. Qualify 2012 2011 [cited 2014 10 May]. Available from: http://dl.geomagic.com/media/marketing/2012_Brochures/MASTER-12_29_11_QQP_A4_English_eVersion.pdf.

19. Besl PJ, McKay ND. A method for registration of 3-D shapes. Pattern Analysis and Machine Intelligence, IEEE Transactions on. 1992;14(2):239-56.

20. Audette MA, Ferrie FP, Peters TM. An algorithmic overview of surface registration techniques for medical imaging. Medical image analysis. 2000;4(3):201-17.

21. Jansson T. Feature Based Registration. January; 2006.

22. Hebert M, Krotkov E, editors. 3-D measurements from imaging laser radars: how good are they? Intelligent Robots and Systems '91 'Intelligence for Mechanical Systems, Proceedings IROS '91 IEEE/RSJ International Workshop on; 1991 3-5 Nov 1991.

23. Huising EJ, Gomes Pereira LM. Errors and accuracy estimates of laser data acquired by various laser scanning systems for topographic applications. ISPRS Journal of Photogrammetry and Remote Sensing. 1998;53(5):245-61.

24. Bao J, Yao YL. Analysis and Prediction of Edge Effects in Laser Bending. Journal of Manufacturing Science and Engineering. 2000;123(1):53-61.

25. Böhler W, Bordas Vicent M, Marbs A. Investigating Laser Scanner Accuracy-The International Archives of Photogrammetry, Remote Sensing and Spatial Information Sciences, Vol. XXXIV, Part. 2003;5:C15.

26. Zeibak R, Filin S. Managing uncertainty in the detection of changes from terrestrial laser scanners data. XXI ISPRS Congress: Commission V, WG 3. Beijing2008.

27. Tang P, Akinci B, Huber D. Quantification of edge loss of laser scanned data at spatial discontinuities. Automation in Construction. 2009;18(8):1070-83.

28. Sanz-Cortiella R, Llorens-Calveras J, Rosell-Polo JR, Gregorio-Lopez E, Palacin-Roca J. Characterisation of the LMS200 laser beam under the influence of blockage surfaces. Influence on 3D scanning of tree orchards. Sensors (Basel, Switzerland). 2011;11(3):2751-72.

29. Loftus G. On interpretation of interactions. Memory & Cognition. 1978;6(3):312-9.

30. Newman I, Newman C. Conceptual statistics for beginners. 2 ed. Lanham, MD: University Press of America; 1994.

31. Stevens. Interaction effects in ANOVA 2004 [cited 2015 3 January]. Available from: http://pages.uoregon.edu/stevensj/interaction.pdf.

32. Andrew DP, Pedersen PM, McEvoy CD. Research methods and design in sport management: Human Kinetics; 2011.

33. Moss JP, Linney AD, Grindrod SR, Moss CA. A Laser Scanning System for the Measurement of Facial Surface Morphology. Optics and Lasers in Engineering. 1989, 10:179-190

34. Motohashi N, Kurdoa T. A 3D computer-aided design system applied to diagnosis and treatment planning in orthodontics and orthognathic surgery. European Journal of Orthodontics. 1999, 21:263-274

35. Bell A, Ayoub AF, Siebert P. Assessment of the accuracy of three-dimensional imaging system for archiving study models. Journal of orthodontics. 2003, 30:219-223

36. Zilberman O, Huggare JV, Parikakis KA . Evaluation of the Validity of Tooth Size and Arch Width Measurements Using Conventional and Three-dimensional Virtual Orthodontic Models. The Angle Orthodontist. 2003, 73(3):301-306

37. Winder RJ, Darvannb TA, McKnightc W, Mageed JDM, Ramsay-Baggs P. Technical validation of the Di3D stereophotogrammetry surface imaging system. British Journal of Oral and Maxillofacial Surgery. 2008, 46:33-37

38. Nouri M, Massudi R, Bagheban AA, Azimi S, Fereidooni . The accuracy of a 3-D laser scanner for crown width measurements. Aust Orthod J. 2009, 25(1):41-47

39. Fleming PS, Marinho V, Johal A , Orthodontic measurements on digital study models compared with plaster models: a systematic review. Orthodontics & Craniofacial Research. 2001, 14(1):1-16

40. El-Katatny I, Masood SH, Morsi YS. Error analysis of FDM fabricated medical replicas. Rapid Prototyping Journal. 2010, 16(1):36-43

41. Macario Alex. Editorial, What does one minute of operating room time cost? Journal of Clinical Anesthesia. 2010. 22: 233-236

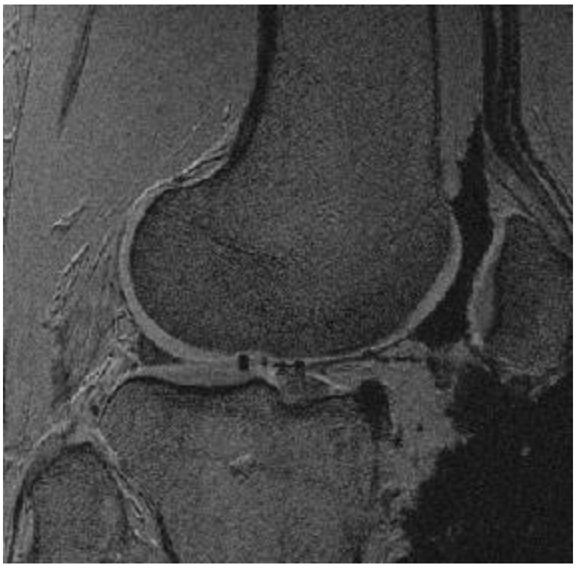

Figure 1: A sample MRI scan of the right knee joint

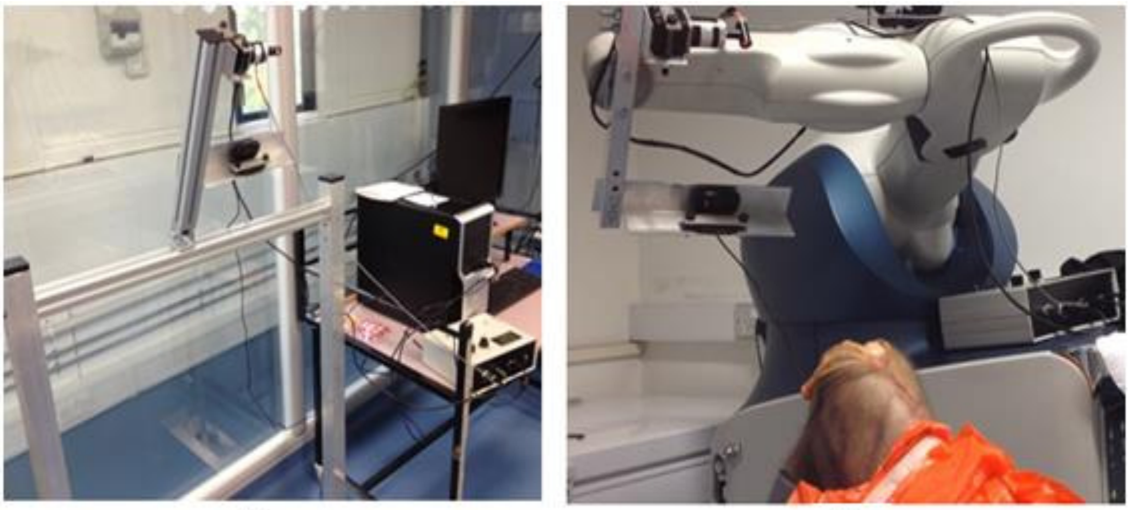

(a) (b)

Figure 2: 3D Laser scanner (a): Scanner mounted on the aluminium extrusion framework (b): Laser scanner mounted on the joint six of the MAKO RIO® arm

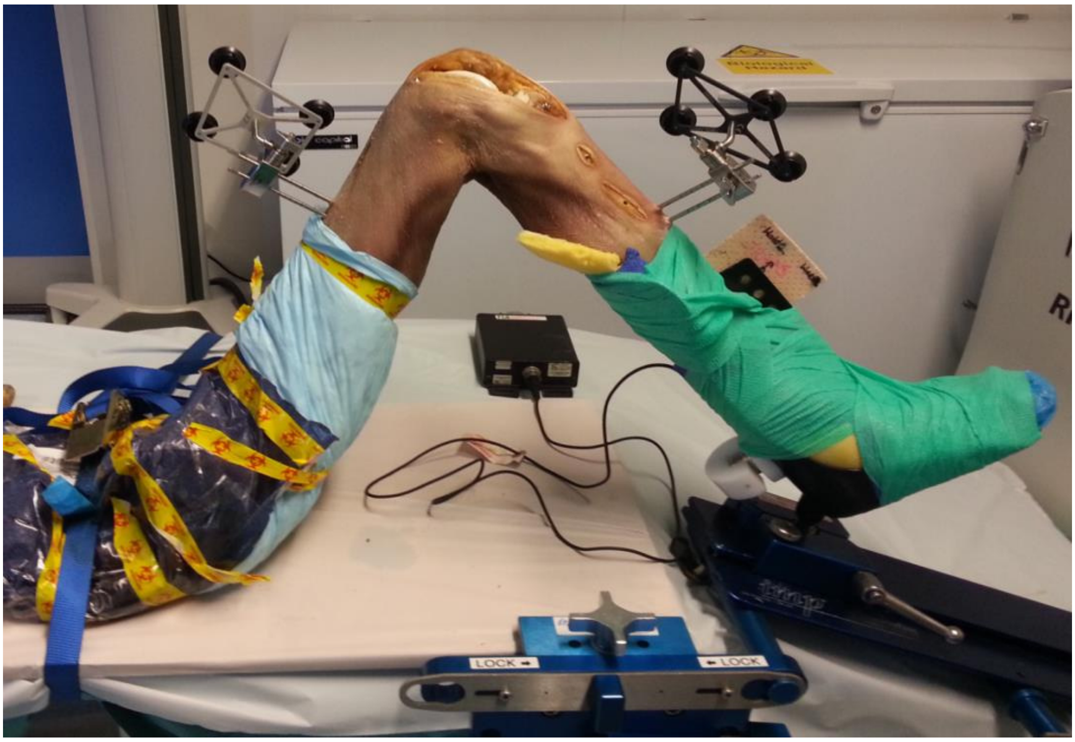

Figure 3: Sample cadaver set up on the bed with the attached arrays for MAKO registration

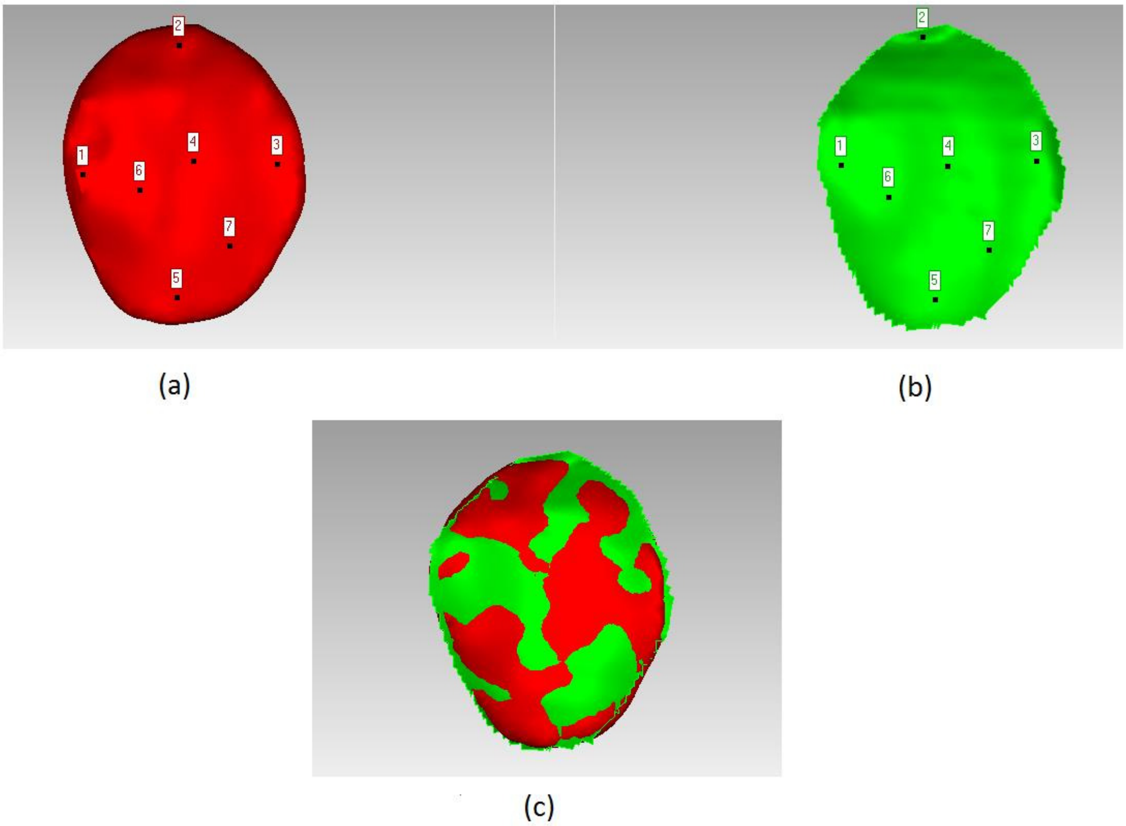

Figure 4: Manual registration by selecting random points over the left lateral tibial surface

(a): MRI generated 3D model (red) of the articular cartilage, set as a reference model. (b): Corresponding 3D laser scan (green) of the same cartilage acquired intra-operatively, set as a test model. (c): Rough manual registration between two surfaces

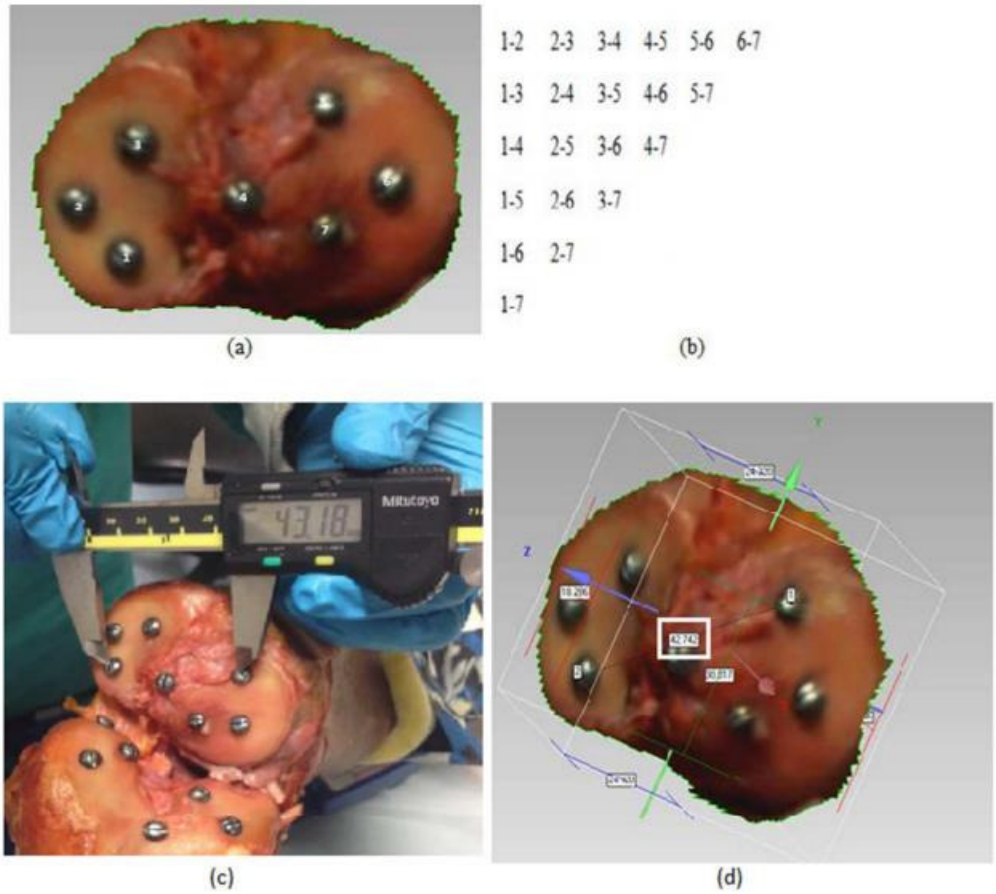

Figure 5: Distance measurements between the screw markers on the tibial condyle (a): Placement of seven screws over the surface (b): Total number of measurements (21) computed between every pair of the points (c): Direct distance measurement acquired using digital vernier calliper (d): Distance measurement (in the white box) acquired on the corresponding digitised 3D laser scan and formulated using Geomagic Qualify®

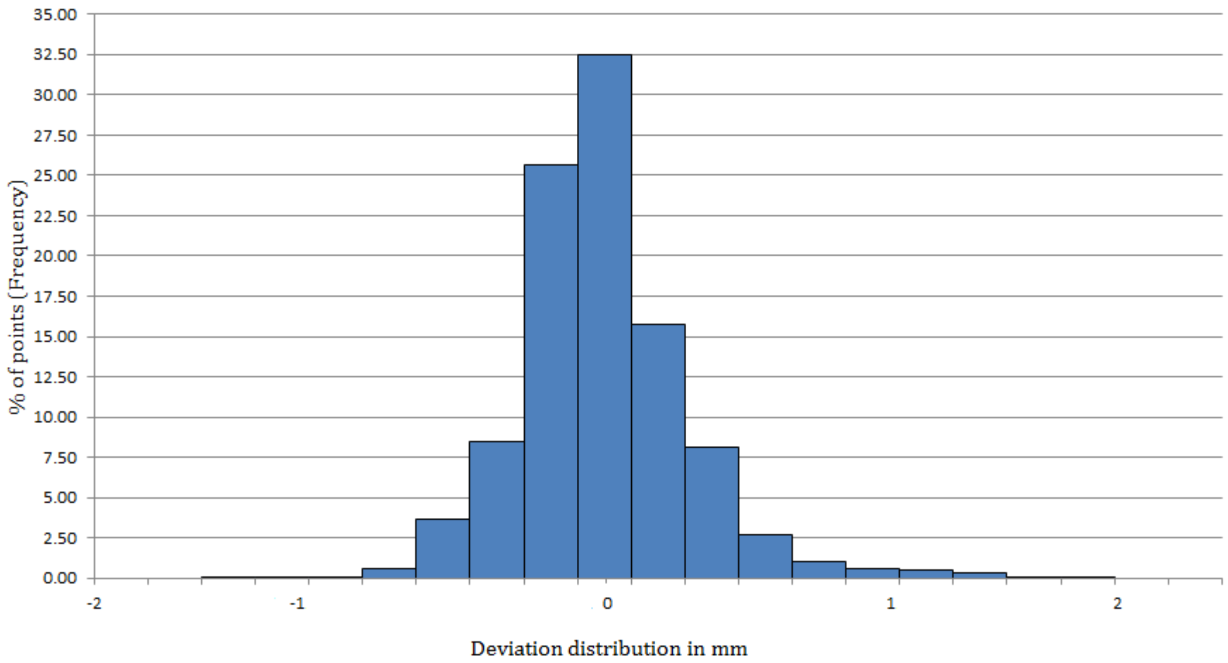

Figure 6: Deviation distribution between MRI and laser scan of an example right femoral lateral cartilage

Deviation in mm is plotted against the percentage of points within the range of deviations. Note: $\pm d_{max}$ occurred at the periphery

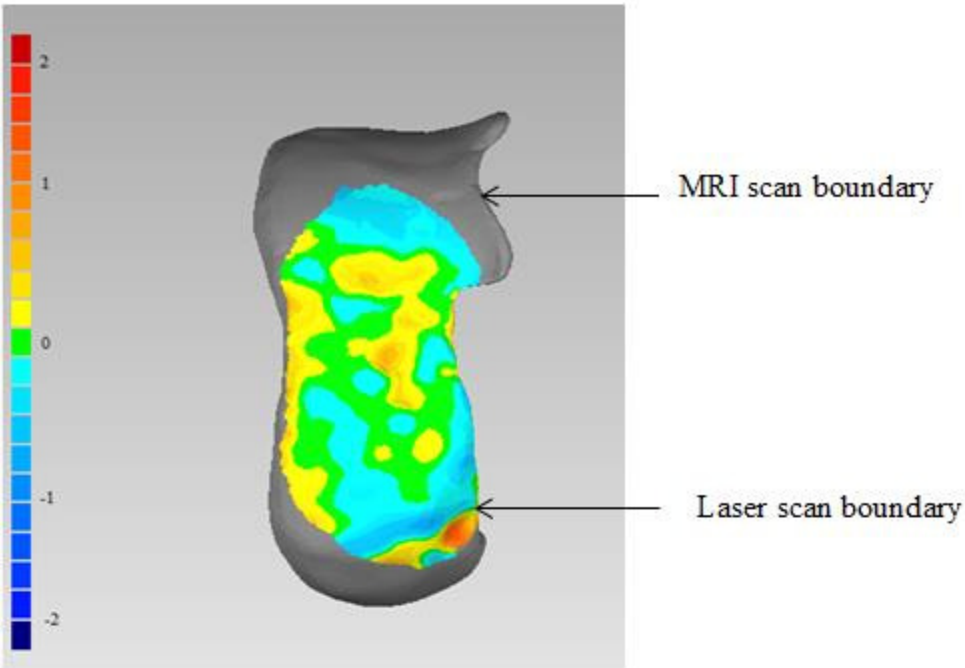

Figure 7: Top view of the colour deviation map showing spatial distribution of the deviations between MRI and laser scan of right femoral lateral cartilage

The posterior and superior condylar region is clipped as the laser scan was acquired with a minimal exposure (90 mm, mimicking UKA). Note: Large errors ($\pm d_{max}$) at the periphery

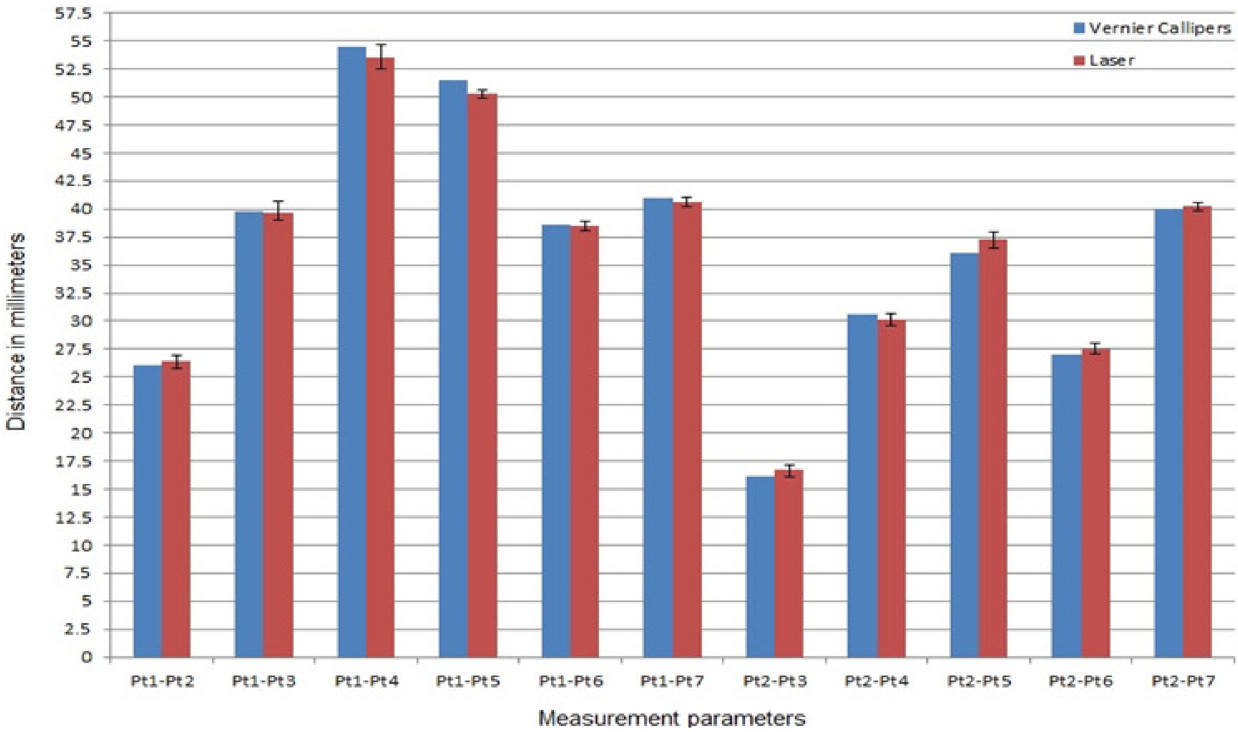

Figure 8: Bar graph for the comparison for the distance calculations between vernier calliper and 3D laser scans

(a): Bar graph for first 11 pairs of screws. (b): Bar graph for remaining 10 pairs of screws

Note: Blue bar is the measurement recorded by the vernier calliper, whereas red bar is the mean value of the measurements on the laser scans. Error bars indicate the range of values (minimum and maximum values). All the measurement differences between vernier calliper and laser were statistically not significant; $P>0.05$

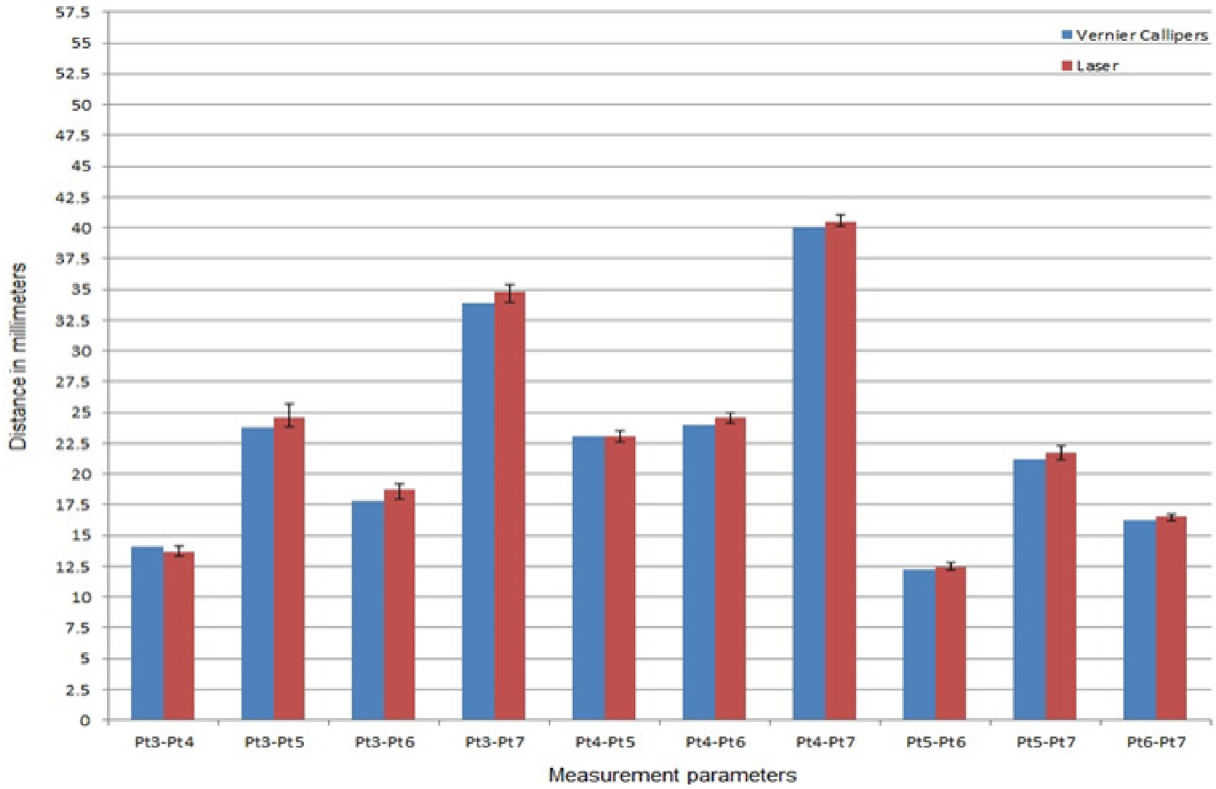

Figure 8: Bar graph for the comparison for the distance calculations between vernier calliper and 3D laser scans

(a): Bar graph for first 11 pairs of screws. (b): Bar graph for remaining 10 pairs of screws

Note: Blue bar is the measurement recorded by the vernier calliper, whereas red bar is the mean value of the measurements on the laser scans. Error bars indicate the range of values (minimum and maximum values). All the measurement differences between vernier calliper and laser were statistically not significant; $P>0.05$